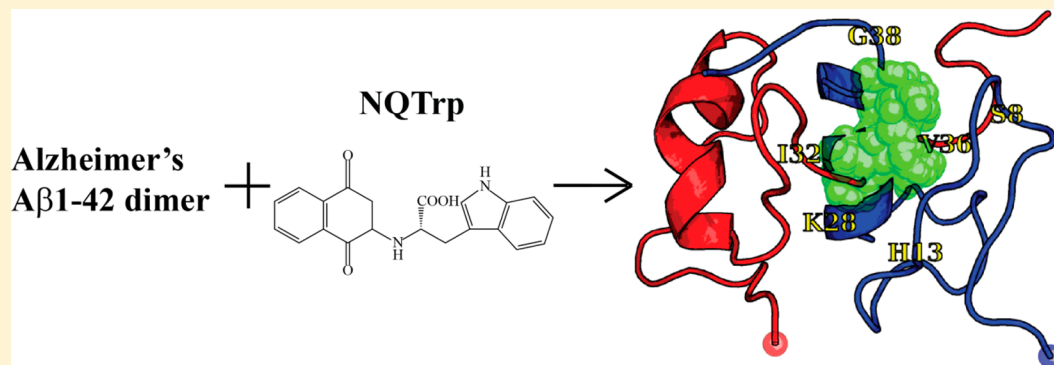


Atomic and Dynamic Insights into the Beneficial Effect of the 1,4-Naphthoquinon-2-yl-L-tryptophan Inhibitor on Alzheimer's A $\beta$ 1–42 Dimer in Terms of Aggregation and ToxicityTong Zhang,<sup>†,‡</sup> Weixin Xu,<sup>‡,§</sup> Yuguang Mu,<sup>\*,‡</sup> and Philippe Derreumaux<sup>\*,†,||</sup><sup>†</sup>Laboratoire de Biochimie Théorique, UPR9080 CNRS, Université Paris Diderot, Sorbonne Paris Cité, Institut de Biologie Physico-Chimique, 13 rue Pierre et Marie Curie, 75005 Paris, France<sup>‡</sup>School of Biological Sciences, Nanyang Technological University, 60 Nanyang Drive, Singapore 637551<sup>§</sup>State Key Laboratory of Precision Spectroscopy, Department of Physics, Institute of Theoretical and Computational Science, East China Normal University, Shanghai 200062, China<sup>||</sup>Institut Universitaire de France, 103 Boulevard Saint-Michel, 75005 Paris, France

## Supporting Information



**ABSTRACT:** Aggregation of the amyloid  $\beta$  protein ( $A\beta$ ) peptide with 40 or 42 residues is one key feature in Alzheimer's disease (AD). The 1,4-naphthoquinon-2-yl-L-tryptophan (NQTrp) molecule was reported to alter  $A\beta$  self-assembly and reduce toxicity. Though nuclear magnetic resonance experiments and various simulations provided atomic information about the interaction of NQTrp with  $A\beta$  peptides spanning the regions of residues 12–28 and 17–42, none of these studies were conducted on the full-length  $A\beta$ 1–42 peptide. To this end, we performed extensive atomistic replica exchange molecular dynamics simulations of  $A\beta$ 1–42 dimer with two NQTrp molecules in explicit solvent, by using a force field known to fold diverse proteins correctly. The interactions between NQTrp and  $A\beta$ 1–42, which change the  $A\beta$  interface by reducing most of the intermolecular contacts, are found to be very dynamic and multiple, leading to many transient binding sites. The most favorable binding residues are Arg5, Asp7, Tyr10, His13, Lys16, Lys18, Phe19/Phe20, and Leu34/Met35, providing therefore a completely different picture from *in vitro* and *in silico* experiments with NQTrp with shorter  $A\beta$  fragments. Importantly, the 10 hot residues that we identified explain the beneficial effect of NQTrp in reducing both the level of  $A\beta$ 1–42 aggregation and toxicity. Our results also indicate that there is room to design more efficient drugs targeting  $A\beta$ 1–42 dimer against AD.

**KEYWORDS:** Alzheimer's disease, amyloid  $\beta$  dimer, NQTrp, replica exchange molecular dynamics simulation

One of the hallmarks of Alzheimer's disease (AD) is the aggregation of amyloid  $\beta$  ( $A\beta$ ) peptides into insoluble amyloid plaques.<sup>1,2</sup> The  $A\beta$  peptide results from the cleavage of the amyloid precursor protein (APP) by the  $\beta$ - and  $\gamma$ -secretases. The predominant  $A\beta$  peptides found in the brain are essentially composed of 40 ( $A\beta$ 1–40) and 42 ( $A\beta$ 1–42) residues.<sup>3,4</sup> The aggregation pathways from unstructured  $A\beta$  peptide monomers to amyloid plaques with cross- $\beta$  structure have been extensively studied at a low-resolution level,<sup>5–8</sup> and there is a growing body of evidence that the low-molecular weight oligomers are the main pathogenic agents in AD.<sup>9,10</sup> Even the  $A\beta$  dimer, the

smallest oligomer, is able to impair the normal functions of neuron cells.<sup>11,12</sup>

Characterizing the  $A\beta$ 1–40/ $A\beta$ 1–42 dimer at the molecular and atomic level is a crucial and important step toward understanding  $A\beta$  aggregation and toxicity. Thus far, only low-resolution experimental data for  $A\beta$  dimer are available. Using ion-mobility mass spectrometry, Bernstein et al. reported a collision cross section of 1256 Å<sup>2</sup> for the  $A\beta$ 1–42 dimer.<sup>13</sup>

**Received:** October 30, 2013

**Revised:** November 18, 2013

**Published:** November 19, 2013

Using different preparation methods and circular dichroism (CD) analysis, Teplow reported a  $\beta$ -strand content between 12 and 25% and an  $\alpha$ -helix content between 3 and 9% at 295 K and pH 7.5 on day 0, for therefore a mixture of various aggregates.<sup>14,15</sup> Experimental characterization of A $\beta$ 1–42 dimer at a higher level of resolution is narrowed because it is strongly aggregation-prone in aqueous solution.<sup>16</sup> In addition, because of its poor solubility, A $\beta$ 1–42 dimer is not suitable for NMR analysis in aqueous solvent.

Computer simulations have been extensively used to provide atomistic-level information about the structures of A $\beta$ 1–40/A $\beta$ 1–42 monomers in aqueous solution<sup>17–20</sup> or A $\beta$ 16–22, A $\beta$ 14–20, or A $\beta$ 18–24 oligomers with inhibitors.<sup>20–22</sup> Several simulations have been conducted on dimers of A $\beta$ 1–40/A $\beta$ 1–42 using various coarse-grained force fields<sup>17,23,24</sup> and all-atom force fields with implicit<sup>25,26</sup> and explicit solvent.<sup>27–30</sup> One common finding is that the interface of A $\beta$ 1–42 dimer is mainly composed of the central hydrophobic core (CHC, residues 17–21) and the C-terminal region (CT, residues 29–42), with predominant CHC–CHC, CT–CT, and CHC–CT interchain interactions, though the contact probabilities vary depending on the force field and conformational sampling method used.<sup>17,26,28–30</sup> Other simulations of larger A $\beta$  aggregates, such as the trimer of A $\beta$ 17–42 peptide using the coarse-grained OPEP force field<sup>31</sup> and 32-mers of the N-terminally truncated A $\beta$ 3–40, A $\beta$ 3–42, A $\beta$ 11–40, and A $\beta$ 11–42 peptides using a square-well coarse-grained force field,<sup>32</sup> have also reported similar binding interfaces. Overall, the interpeptide interface in A $\beta$ 1–42 dimer and oligomers mainly involves the CHC and CT regions and is independent of the force field used.

Finding an effective inhibitor of A $\beta$  oligomerization is an important step in the treatment of AD. In the past decade, many molecules have been shown to inhibit A $\beta$  oligomerization *in vitro* and reduce toxicity in cell assays. These include (1) proteins, such as *Escherichia coli* maltose binding protein (MBP);<sup>33</sup> (2) short peptides, such as the “Ghanta peptide”<sup>34</sup> and “Soto peptide”;<sup>35</sup> (3) fragments of A $\beta$  peptides, such as KLVFF,<sup>36</sup> or fragments spanning the C-terminal region;<sup>37</sup> (4) chemical compounds extracted from natural products, such as EGCG from green tea<sup>38</sup> and curcumin from cinnamon;<sup>39</sup> and (5) synthetic compounds, such as the 1,4-naphthoquinon-2-yl-L-tryptophan (NQTTrp),<sup>40</sup> based on the inhibitory capability of naphthoquinone on A $\beta$  oligomerization<sup>41</sup> and the strong amyloidogenic potential of tryptophan.<sup>42</sup>

The structure of NQTTrp is shown in Figure 1A. Experimentally, NQTTrp has been reported to reduce the toxicity of A $\beta$  oligomers and completely recover the phenotype on a transgenic AD *Drosophila* model.<sup>40</sup> Its inhibition effect has also been discussed with respect to other amyloidogenic peptides, such as  $\alpha$ -synuclein, islet amyloid polypeptide, and calcitonin.<sup>43</sup> The NMR structure of A $\beta$ 12–28 monomer determined in the presence of a 0.25 molar ratio of NQTTrp to A $\beta$ 12–28 showed the most prominent interactions in the region of residues 18–24.<sup>40</sup> All-atom implicit solvent molecular dynamics (MD) simulations using the CHARMM/CMAP force field of A $\beta$ 12–28 monomer with one single NQTTrp molecule reported there are no predominant binding modes, although NQTTrp preferentially interacts with residues His13–Phe20 through its carboxyl group (labeled 15–17 in Figure 1A) and two aromatic moieties (labeled 1–12 for naphthoquinone and 19–27 for indole in Figure 1A).<sup>44</sup> Replica exchange molecular dynamics (REMD) simulation using the coarse-

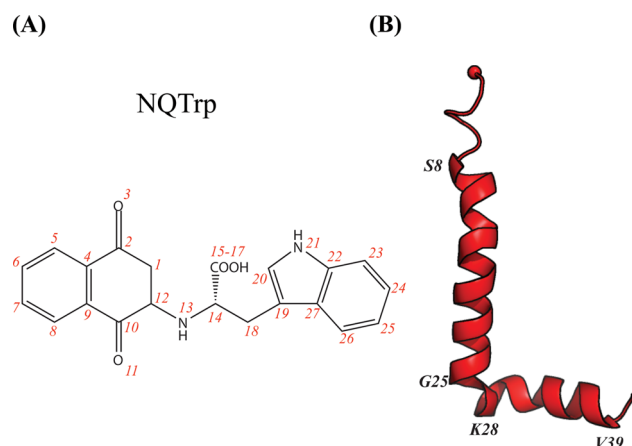


**Figure 1.** Structures of the NQTTrp molecule and A $\beta$  monomer. (A) Chemical structure of the NQTTrp molecule. The red numbers label all the heavy atoms. (B) Initial A $\beta$  conformation. The red sphere represents the C $\alpha$  atom of Asp1.

grained OPEP force field followed by all-atom docking calculations also marked the NQTTrp molecule as the best binder to A $\beta$ 17–42 trimeric structures among five small-molecule drugs. These simulations also showed that NQTTrp has multiple binding modes with different affinities, although it interacts preferentially with the CHC region. Finally, all-atom implicit solvent MD simulations of the trimers of A $\beta$ 14–20, A $\beta$ 16–22, and A $\beta$ 18–24 peptides with one single NQTTrp molecule and NQTTrp derivatives emphasized the role of Phe19 and Phe20 side chains and the anilic NH group of NQTTrp (labeled as 13 in Figure 1A) in binding.<sup>22</sup> Overall, although these simulations provide mechanistic insight into the activity of NQTTrp on A $\beta$  fragments, how NQTTrp interacts with the full-length A $\beta$  protein remains to be determined.

To this end, we performed all-atom simulations of A $\beta$ 1–42 dimer with two NQTTrp molecules. To overcome the sampling issue, we used REMD simulation in explicit solvent with 64 replicas between 315 and 450 K. Our previous REMD study of A $\beta$ 1–42 dimer in the absence or presence of 10 EGCG molecules demonstrated it is an efficient way to study A $\beta$ 42 dimer–inhibitor interactions.<sup>30</sup> Our aim in this study is to provide an atomic picture of the modes of action of NQTTrp on A $\beta$ 1–42 dimer to improve our understanding of its inhibitory mechanism on A $\beta$  oligomerization and toxicity.

## RESULTS

**Convergence.** The simulation convergence was assessed by several criteria. As shown in Figure 2A, one representative replica visits a wide range of temperatures over 250 ns, indicating an efficient walk in temperature space. The conformational entropy at the lowest temperature, 315 K, shown in Figure 2B, remains relatively constant after 150 ns. The coil, turn,  $\alpha$ -helix, and  $\beta$ -strand contents of the peptides as a function of temperature are shown in panels C–F, respectively, of Figure 2, using three different time intervals, 100–150, 150–200, and 200–250 ns. The superposition of the curves for 150–200 and 200–250 ns indicates that the propensities for the four secondary structures have converged. The high degree of similarity of the  $\alpha$ -helical propensity profiles among the three regimes clearly demonstrates that the memory of the originally assumed structure does not play any role. The coil propensity as a function of the amino acids for the three

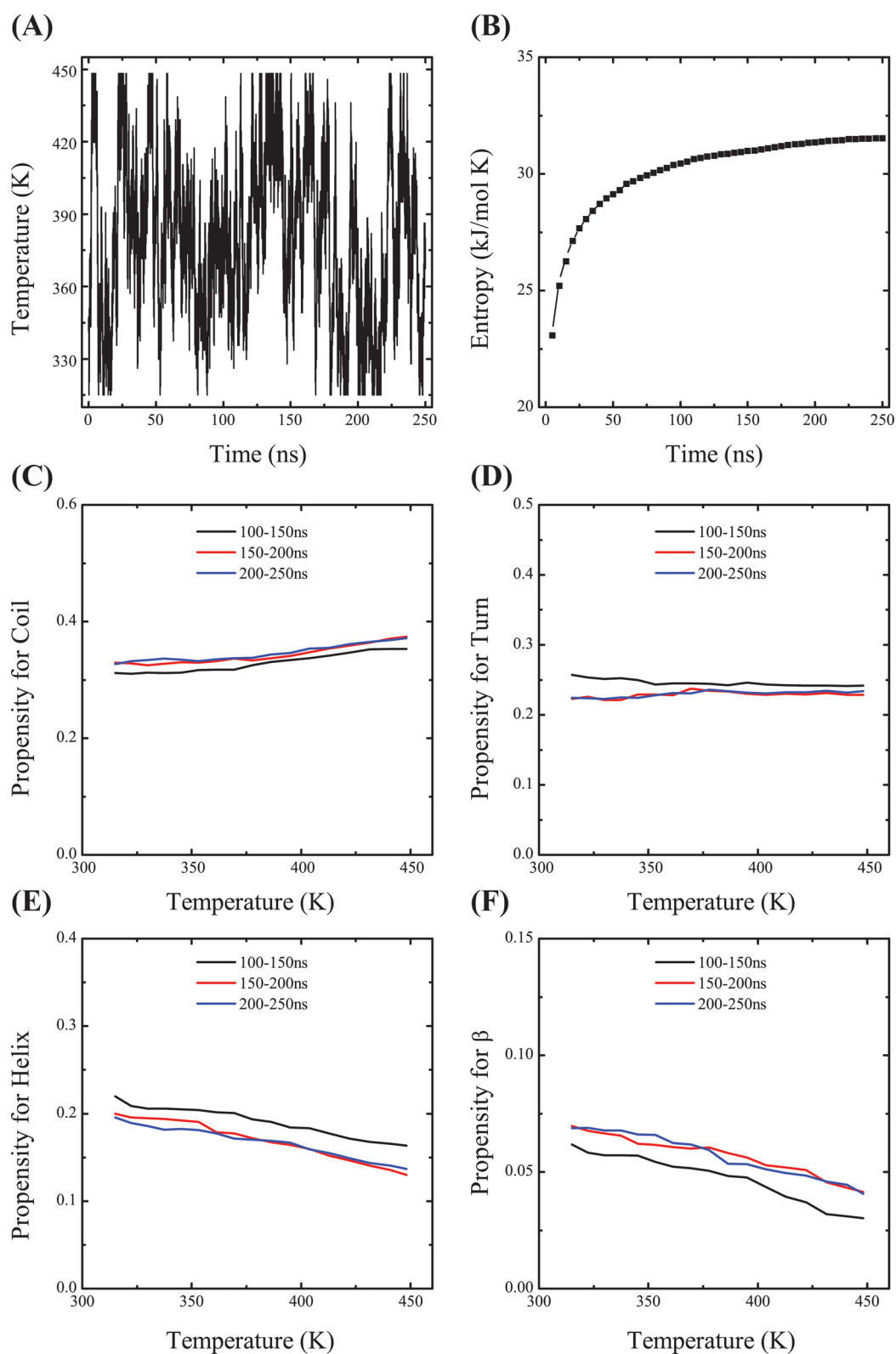


**Figure 2.** Simulation convergence. (A) Time evolution of one replica in temperature space. (B) Time evolution of the conformational entropy as estimated by the quasi-harmonic approach based on the ensemble trajectory at 315 K. (C) Propensity of coil as a function of temperature in the time intervals of 100–150, 150–200, and 200–250 ns. (D) Propensity of turn as a function of temperature in the three time intervals. (E and F) Propensities of  $\alpha$ -helix and  $\beta$ -strand, respectively, as a function of temperature in the three time intervals.

time intervals is shown in Figure 3A. The percentage of coil for each amino acid remains constant as the simulation progresses from 100 to 250 ns. The fraction of exposed side chain surface area for each amino acid, shown in Figure 3B, does not vary

from one time interval to another. The inter-center-of-mass distance between the two  $A\beta$  peptides at 315 K is monitored in Figure 4A. During the first 100 ns, the  $A\beta$  peptides approach gradually and then remain at a distance of

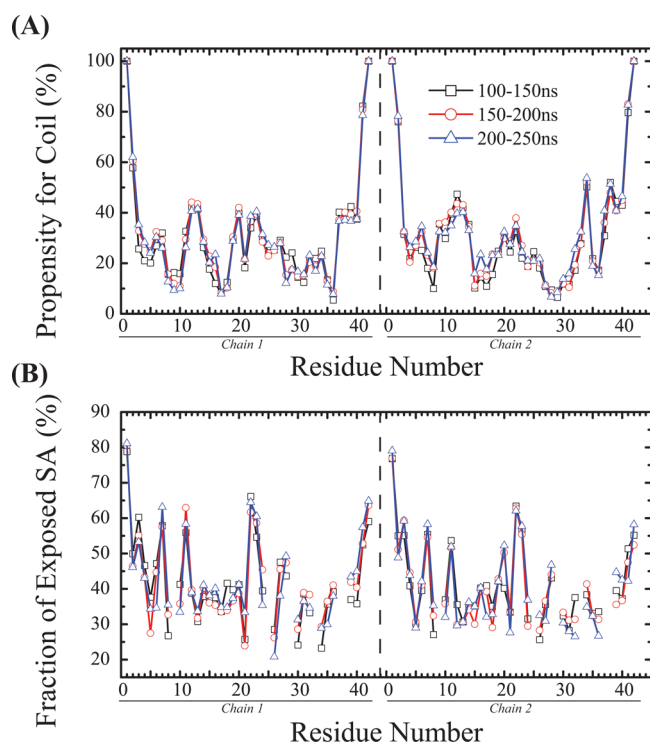


**Figure 3.** Per-residue convergence assessment. (A) Coil propensity of each Aβ residue at 315 K and (B) fraction of exposed side chain surface area at 315 K using the three time windows. Note the curves are discontinuous at glycine.

1.2 nm in the following 150 ns. Figure 4B shows the time evolution of the total number of heavy atom contacts between the two Aβ peptides at 315 K. The number of contacts increases during the first 100 ns and then fluctuates around 1000 during the 100–250 ns period. Taken together, all these results indicate that the conformational ensemble has reasonably converged within 250 ns. In what follows, analysis is based on the ensemble trajectory at 315 K from 100 to 250 ns.

**Two-Dimensional Structures and Contact Maps of Aβ Dimer.** Averaged over the two peptides, the secondary structure propensities at 315 K show that coil is the most populated ( $32.0 \pm 1.0\%$ ) and β-strand is the least populated ( $6.8 \pm 0.9\%$ ). Bend, turn, and α-helix have populations of  $17.5 \pm 0.4$ ,  $24.2 \pm 1.5$ , and  $19.5 \pm 0.7\%$ , respectively. Via examination of the per-residue secondary structure propensity, in Figure 5, the β-strand content is mainly observed in the CT region (12%) and then in the CHC (8%) and NT (3.8%) regions. The α-helix content is observed at residues 12–18 (32%), residues 30–35 of the CT region (22%), and the FL region (19%).

The Aβ dimer interface is assessed by the weak intermolecular side chain–side chain contact map, as seen in Figure 6. The interface is characterized by CT–CT interactions among residues 30–35 with a lifetime probability of  $8.4 \pm 0.2\%$ , and the strongest interaction between residues Ile31 and Leu34 has a lifetime of 27%. The CT–CHC interactions have a lifetime probability of  $5.1 \pm 0.7\%$  using residues 30–35 for CT, and the strongest interaction between Phe19 and Ile38 has a lifetime of 18%. The CHC–CHC interactions have a lifetime probability of  $3.3 \pm 0.3\%$ , and the strongest interaction between Phe19 and Phe20 has a lifetime of 12%. In contrast, the intra-

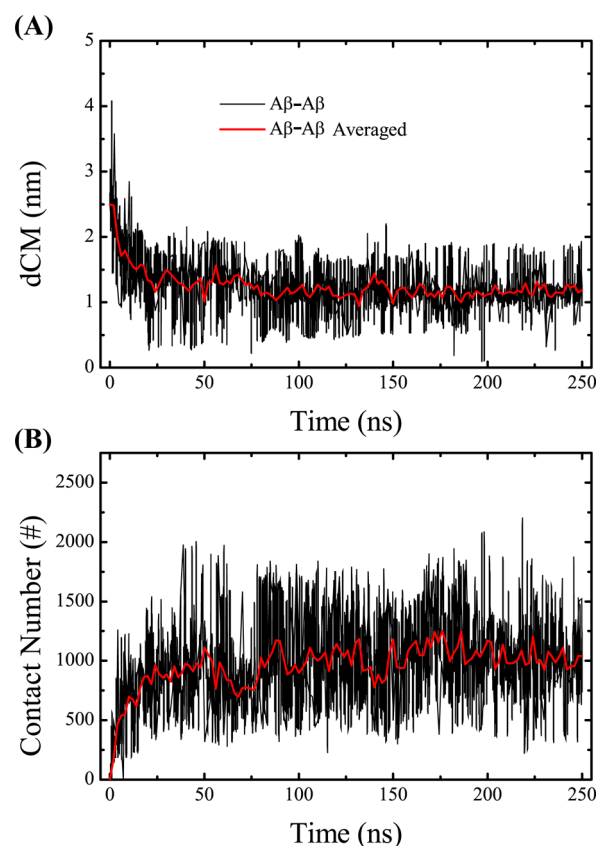


**Figure 4.** Time evolution of two global properties of Aβ dimer. (A) Time evolution of the inter-center-of-mass distance, dCM, between the two Aβ peptides (gray) and the averaged value (red). (B) Time evolution of the total number of heavy atom contacts between the Aβ peptides (gray) and the averaged value (red).

and intermolecular interactions between NT and the rest of the protein are almost negligible.

**Binding of NQTrp to Aβ Dimer.** The distribution of NQTrp molecules around the Aβ dimer is assessed by the radial distribution function (RDF) shown in Figure 7. The RDF and the height of the peak at 0.36 nm from Aβ1–42 dimer surface indicate direct binding of NQTrp to Aβ peptides. For a system containing two Aβ peptides and two NQTrp molecules, six different states for characterizing the binding exist. These states can be defined as P1 (all peptides and NQTrp are separated), P2 (one Aβ interacts with one NQTrp), P3 (one Aβ interacts with two NQTrp molecules), P4 (the two peptides interact with each other, but not with NQTrp), P5 (the two peptides interact with each other and with one NQTrp, whereas the second NQTrp is devoid of any intermolecular interactions), and P6 (the two peptides interact with each other and with the two NQTrp molecules). Using all conformations within the time frame of 100–250 ns at 315 K, the population of the P1–P3 states is 0%, indicating the absence of free Aβ monomers. The population of the P4 state is also 0%, indicating no dimers free of NQTrp. The populations of the P5 and P6 states are  $1.7 \pm 0.2$  and  $98.3 \pm 0.2\%$ , respectively, indicating that most of the conformational ensemble is characterized by two Aβ peptides forming a dimer and interacting with both NQTrp molecules. Via examination of the P6 heterotetramer interactions, the most dominant binding mode ( $59.2 \pm 0.2\%$ ) is described by the two NQTrp molecules interacting and intercalated between both peptides. The second

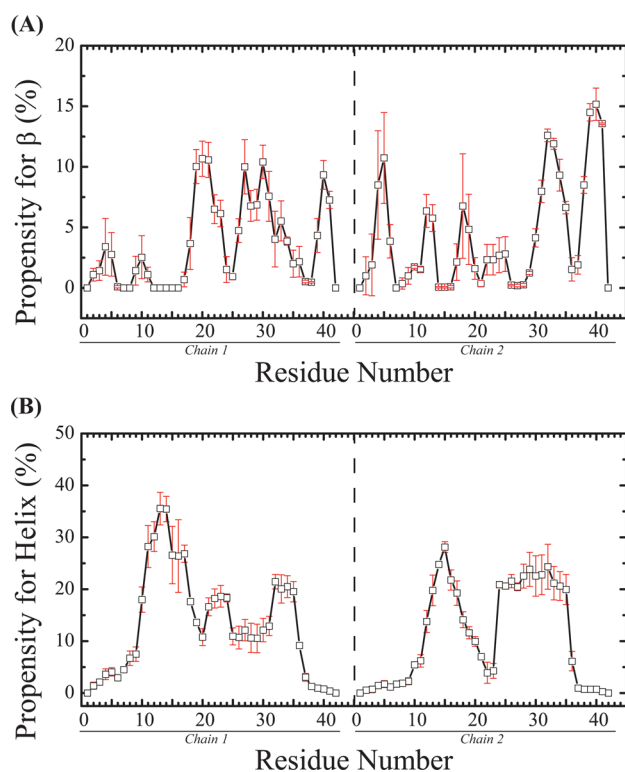


**Figure 5.** Secondary structure propensities of each amino acid at 315 K: (A)  $\beta$ -strand and (B)  $\alpha$ -helix. The vertical dashed line separates the two chains. The error bars represent the standard errors estimated by block averaging.

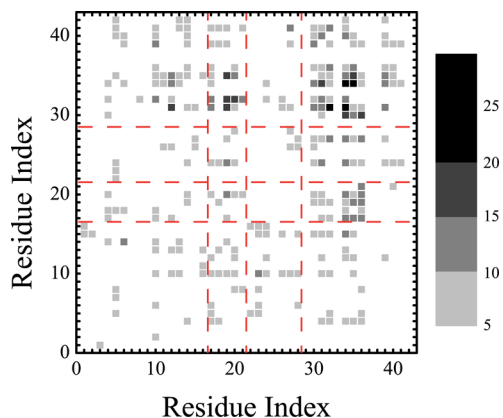


**Figure 6.** Interpeptide side chain-side chain contact maps. The color scale defines the contact probability. The red dashed lines define the four  $A\beta$  regions: NT, CHC, FL, and CT.

state ( $33.5 \pm 0.1\%$ ) has one NQTrp interacting with both peptides, whereas the second NQTrp interacts with only one  $A\beta$ ; finally, the third state ( $7.3 \pm 0.1\%$ ) is such that one NQTrp interacts with one single  $A\beta$ .

The binding of NQTrp to  $A\beta$ 1–42 dimer can be further examined by the contact maps between the heavy NQTrp atoms and the heavy  $A\beta$  main chain and side chain atoms shown in panels A and B of Figure 8, respectively. The carboxyl group (atoms 15–17) of NQTrp displays a larger number of contacts with the main chain atoms of  $A\beta$  peptides than the other atoms (Figure 8A). The same carboxyl group and the outward atoms of the two aromatic moieties of NQTrp (atoms 3 and 5–8 from naphtoquinone and atoms 25 and 26 from

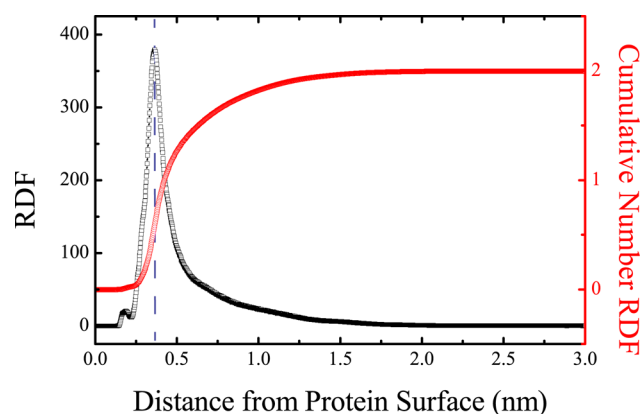


**Figure 7.** Radial distribution functions of NQTrp from  $A\beta$  dimer. The RDF is shown with black squares. The cumulative number RDF is shown with red circles. The vertical blue dashed line labels the position of the highest peak in the RDF curve.

indole) also form roughly 25% more contacts with the side chain atoms of  $A\beta$  than the other atoms. The main chain atoms of residues Met35/Leu34, Gly37/Gly38, Gly9/Tyr10, Gly29, Ser26, Lys16, and Arg5 interact strongly with NQTrp (Figure 8A), while the side chain atoms of residues Phe4/Arg5, Tyr10, His13, Lys16, Phe19/Phe20, Ile31/Ile32, and Leu34/Met35 interact preferentially with NQTrp (Figure 8B). The H-bond propensity between the  $A\beta$  amino acids and NQTrp, shown in Figure 9A, reveals that residues Glu3, Arg7, Ser8, Glu11, Glu22, Asp23, Gly29, and Ala30 have a probability of forming H-bonds with NQTrp of 6–8%. The other residues except residues Asp1, Ala2, Glu11, Ala21, Val24, Ile31/32, Val36, Gly38, and Ile41 have a H-bond probability of 2–6%. As expected, residues Gly29 and Ala30 form backbone H-bonds with NQTrp, while residues Glu3, Arg7, Ser8, Glu11, Glu22, and Asp23 form H-bonds with NQTrp mainly by their side chains. Figure 9B–F also shows the H-bond propensity between the CO (NH) atoms of NQTrp and the main chain and side chains of  $A\beta$ , revealing the heterogeneity of the interactions, even if CO atoms 10 and 11 of naphtoquinone show a much lower H-bond propensity than NH atoms 13 and 21 and COOH atoms 15–17.

The strength of the interaction between NQTrp and each  $A\beta$  residue can be estimated by the molecular mechanics/Poisson–Boltzmann surface area (MM/PBSA) method. The total interaction free energies between NQTrp and each amino acid, as well as the contributions from van der Waals interactions, electrostatic interactions, and solvation, are shown in Figure 10. As seen in Figure 10A, all  $A\beta$  residues display a favorable interaction ( $<0$  kcal/mol), but 10 residues, Tyr10, Leu34/Met35, Arg5, Lys16, Asp7, His13, Lys28, and Phe20/Phe19, are the most favorable binding partners. The favorable interaction free energies between NQTrp and residues Tyr10, Leu34, Met35, and Phe20/Phe19 result mainly from van der Waals interactions and solvation (Figure 10B,D). The favorable interaction free energy between NQTrp and Arg5 comes mostly from van der Waals interactions, while the favorable interaction free energy between NQTrp and Lys16 and Asp7 results from electrostatic interactions (Figure 10C).

Finally, to predict the binding pockets of NQTrp on  $A\beta$ 1–42 dimer, the  $A\beta$ 1–42 configurations were clustered, and the representative structures of the first 10 most populated clusters are shown in Figure 11. The population of each cluster is shown in Table 1. The first cluster displays two  $\alpha$ -helices

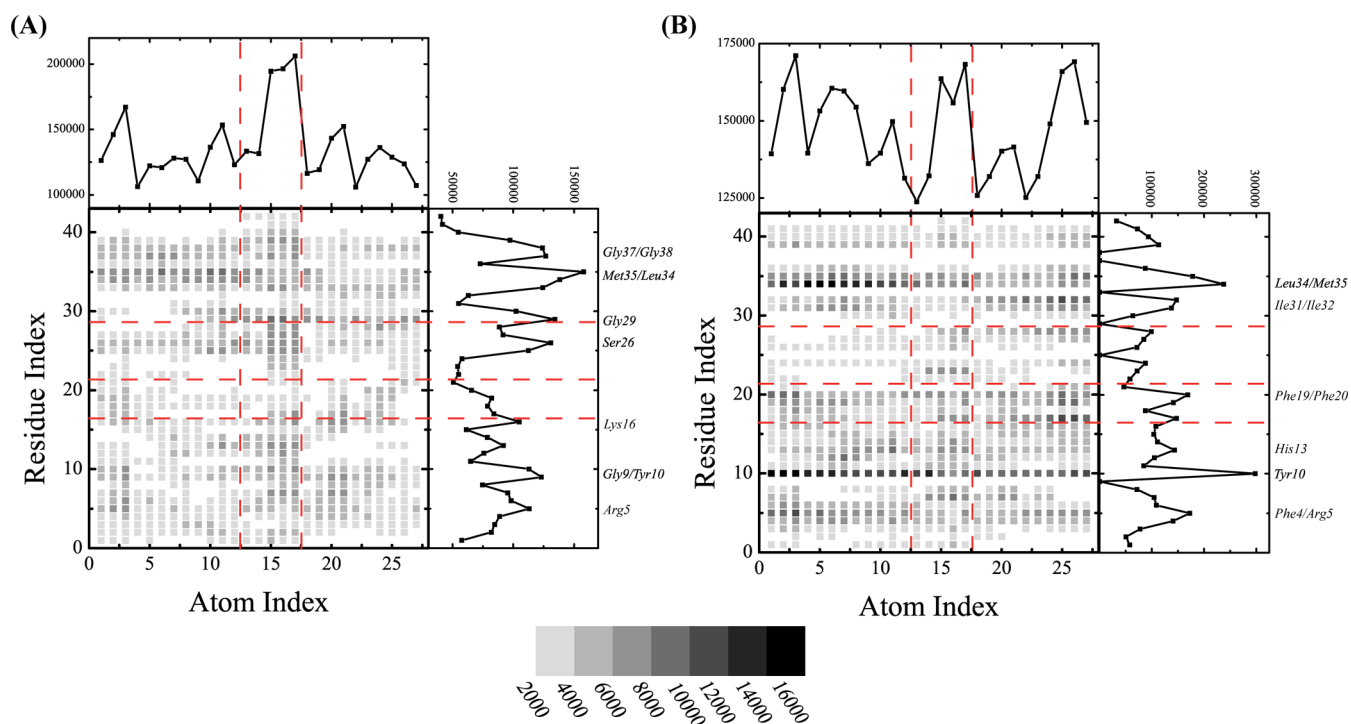


**Figure 8.** Contact maps between the heavy atoms of NQTrp and  $A\beta$ 1–42 residues. (A) Interactions with the backbone  $A\beta$  atoms. (B) Interactions with the side chain  $A\beta$  atoms. The labeling of the NQTrp heavy atoms is shown in Figure 1A. The color scale reflects the number of contacts. The cumulative number of contacts for each heavy atom of NQTrp and  $A\beta$  is shown in the top panels and right panels, respectively. Amino acids with a large number of contacts are labeled. The red dashed lines label the naphthoquinone, peptide bond, and indole groups of NQTrp from left to right on the  $x$ -axis, and the four  $A\beta$  regions (NT, CHC, FL, and CT) on the  $y$ -axis from bottom to top, respectively.

spanning the CHC or part of CT (residues 30–35) region in each chain. The second cluster is essentially random coil with two short helices of residues 3–6 in one chain and residues 24–28 in the other chain. Cluster 3 shows two  $\alpha$ -helices for residues 13–17 in both chains, while cluster 4 is characterized by four short helices spanning the CHC and FL regions in both chains. Cluster 5 displays two long  $\alpha$ -helices spanning residues 24–36 in one chain and residues 13–21 in the second chain, as well as a short helix at residues 26–28 in the second chain. Cluster 6 is similar to cluster 5, but with only one long helix spanning residues 6–20 in the second chain. Cluster 7 shows one long  $\alpha$ -helix spanning residues 13–25 and one short helix spanning residues 31–34 in one chain, and two short helices spanning residues 17–24 and 32–35 in the second chain. Cluster 8 features a  $\beta$ -hairpin formed by residues 32–34 and 37–40 of one chain packed against a third strand formed by residues 39–41 of the other chain. Cluster 8 also displays four short helices spanning the flanking CHC amino acids in both chains. Cluster 9 is similar to clusters 5 and 6 and is characterized by a long helix spanning residues 24–36 in one chain and two short helices spanning residues 13–15 and 26–32 in the second chain. Finally, cluster 10 displays a long  $\alpha$ -helix spanning residues 11–24 in one chain packed against a random coil second chain. The binding residues to NQTrp in the first 10  $A\beta$ 1–42 clusters are listed in Table 1. The key residues involved in the fifth, sixth, and ninth binding sites are rather similar, differing by several residues, while the other sites are different. Table S1 of the Supporting Information gives the binding residues in the 11–20  $A\beta$ 1–42 clusters. We find there are eight different binding pockets in the first 10 clusters and 15 in the first 20 clusters, which include 29.2 and 46.3% of all  $A\beta$ 1–42 configurations, respectively. Overall, 555 clusters are

found for  $A\beta$ 1–42 dimer, with the first 50 and 100 clusters including 69.8 and 82.6% of the configurations, respectively, and the number of binding pockets is on the same order of magnitude.

## DISCUSSION

Experimentally, NQTrp has been reported to reduce the level of aggregation and toxicity of  $A\beta$ 1–42.<sup>40</sup> In the NMR study of the  $A\beta$ 12–28 monomer with various NQTrp: $A\beta$  molar ratios reported strong amide proton chemical shift changes at Phe20, Ala21, and Glu22 and smaller variations at Val18 and Val24. All-atom MD in implicit solvent showed three dominant binding sites between NQTrp and the  $A\beta$ 18–21 region.<sup>34</sup> Following MD simulations in explicit solvent of  $A\beta$ 12–28 monomer with NQTrp<sup>38</sup> and  $A\beta$ 14–20,  $A\beta$ 16–22, or  $A\beta$ 18–24 trimers with one single NQTrp<sup>39</sup> revealed that the most frequently observed intermolecular contacts involve mainly the region of residues 13–20 with the side chains of Phe19 and Phe20 constituting the site of highest interaction probability and providing therefore the most favorable van der Waals energy. Our total interaction free energies and van der Waals energies using the MM/PBSA method show that the most favorable binding partners are residues Tyr10, Leu34/Met35, Arg5, Lys16, Asp7, Phe20/Phe19, Lys28, and His13, providing therefore a binding picture different from that from the studies with short fragments. After the addition of the information about the highest H-bond interaction probability to our analysis, the preferred binding of NQTrp to  $A\beta$  is in the region of residues 3–35, not only the region of residues 13–20. At the molecular level, our analysis indicates that the dominant binding mechanism with a population of 59% at 315 K involves the two  $A\beta$  peptides interacting together and simultaneously

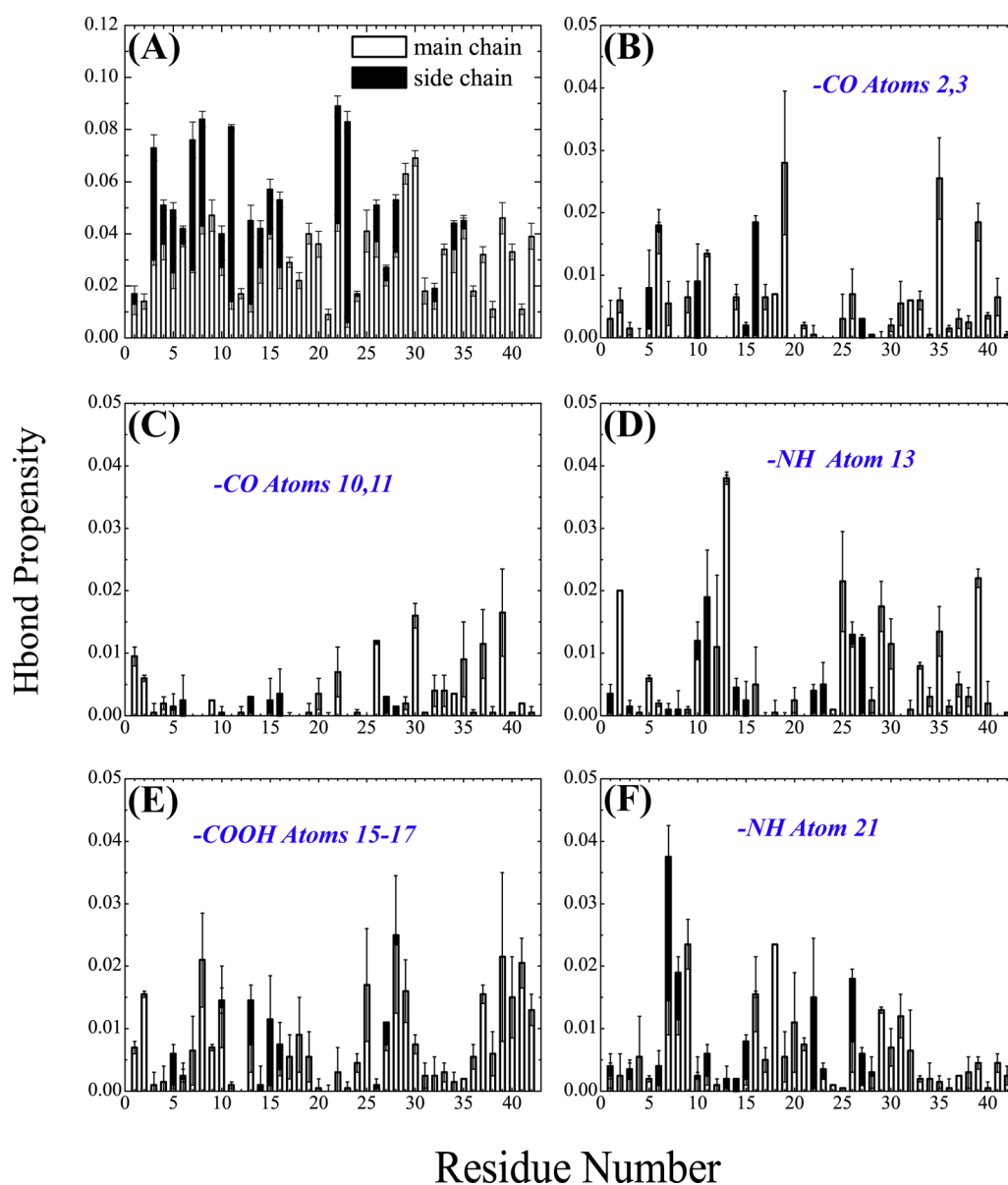


**Figure 9.** H-Bond propensities between  $A\beta$  amino acids and NQTrp. (A) Propensities between NQTrp and the main chain and side chain atoms of  $A\beta$  peptides are shown with white and black bars, respectively. (B–F) Propensities between NQTrp functional groups and the main chain and side chain atoms of  $A\beta$  peptides are shown as white and black bars, respectively.

with the two NQTrp molecules. Although there are multiple binding modes of action, the analysis of intermolecular contact maps shows the NQTrp molecule binds strongly to the CHC and FL regions, reducing therefore the strength of the interpeptide interactions among residues 16–35, interactions that are seen in many simulations of  $A\beta$ 1–40 and  $A\beta$ 1–42 dimers in the absence of inhibitors.<sup>17,25–32,45</sup> Our result is also in agreement with a recent hydrogen–deuterium exchange coupled with mass spectrometry study showing that the region of residues 20–35 is the first to aggregate, followed by the region of residues 36–42 and then the region of residues 1–19 during  $A\beta$ 1–42 oligomerization.<sup>46</sup>

At the residual and atomic level, we have determined that the NQTrp molecules bind mostly to the side chains of residues Arg5, Asp7, Tyr10, His13, Lys16, Phe19/Phe20, Lys28, and Leu34/Met35. All the residues that we identify are known to play very important roles in both  $A\beta$ 1–42 aggregation and toxicity.

Triple substitution of Arg5, Lys16, and Lys28 with Ala results in a significant loss of  $A\beta$ 1–40 fibril toxicity in human embryonic kidney cells.<sup>47</sup> Using CD and fluorescence spectroscopy, transmission electron microscopy, a reactive oxygen species (ROS) fluorescent assay, and neuronal cell viability, mouse  $A\beta$ 1–42 as a three-site mutant (Arg5Gly, Tyr10Phe, and His13Arg) of human  $A\beta$ 1–42 alters the metal copper and zinc binding sites, reduces the likelihood of forming  $\beta$ -sheet structures and aggregated fibrils, alleviates the generation of ROS, and decreases toxicity.<sup>48</sup> Binding of NQTrp to Arg5, Tyr10, and His13 should, therefore, reduce the level of metal binding and toxicity.

The Asp7Asn mutation alters the self-assembly and increases the toxicity of  $A\beta$ 1–40 and  $A\beta$ 1–42 peptides.<sup>49</sup> Binding of NQTrp to Asp7 should therefore reduce both the level of assembly and toxicity.

The Lys16Ala mutation impacts  $A\beta$  self-assembly and dramatically reduces the toxicity of  $A\beta$ 1–40 and  $A\beta$ 1–42

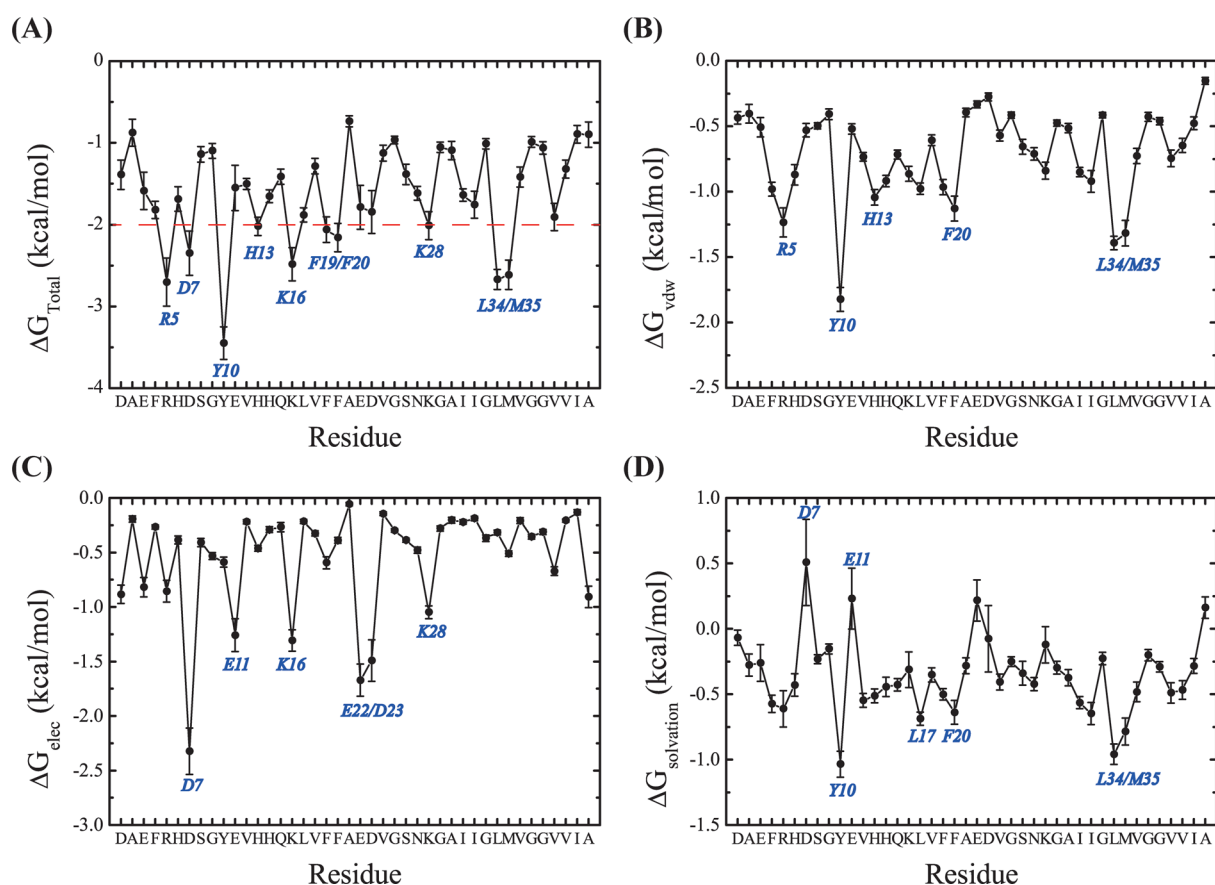


**Figure 10.** Interaction free energies between NQTrp and each  $A\beta$  amino acid. (A) Total interaction free energies. (B) Contribution of van der Waals interactions. (C) Contribution of electrostatic interactions. (D) Contribution of solvation.

peptides.<sup>50</sup> A novel familial  $A\beta$  Lys16Asn peptide has been discovered. The peptide itself is not harmful to neuronal cells, but toxicity is observed for a mixture of  $A\beta$  K16N and its wild-type (WT) counterpart.<sup>51</sup> All-atom MD simulations of both  $A\beta$ 1–40 and  $A\beta$ 1–42 WT and D7N dimers found an interplay between the Asp1–Arg5 and Asp1–Lys16 salt bridges upon introduction of the D7N mutation.<sup>24</sup> Other studies suggested Lys16 is exposed to solvent and interacting with other monomers in  $A\beta$  aggregation.<sup>52–54</sup> We find that the side chain of Lys16 is 47% of the time exposed to the solvent, thereby limiting partially interactions with free monomers during  $A\beta$  oligomerization (Table S2 of the Supporting Information). The formation of the Asp23–Lys28 salt bridge is also known to accelerate fibril formation. We find that Lys28 is 63% of the time accessible to solvent and the intramolecular Glu22–Lys28 and Asp23–Lys28 salt bridges are formed  $7.0 \pm 2.3\%$  and  $9.4 \pm 1.2\%$  of the time, respectively (Table S3 of the Supporting Information).

Using mutagenesis, Leu34 was found to be a key residue for  $A\beta$ 42 aggregation, the Leu34Cys mutation leading to the disruption of hexamer and tetramer formation.<sup>55</sup> In addition, Leu34 is found to be packing with Phe19 in both oligomer and fibril models.<sup>56</sup> We find that the side chain of Leu34 is exposed only 39% of the time to solvent, and the binding of NQTrp prevents Leu34 from interacting with Phe19. Finally, the substitution of Met35 with Val was found to accelerate the kinetics of aggregation of  $A\beta$ 42, and the presence of Met35 is not important for toxicity.<sup>57</sup> We find that the side chain of Met35 is exposed to solvent 42% of the time.

Taken together, our results indicate that the reduced level of  $A\beta$ 1–42 oligomerization and toxicity induced by NQTrp binding results from a multifactorial mechanism. It is also of interest to determine the extent to which our results compare with three recent simulations of  $A\beta$ 1–42 with other small compounds.

In the REMD simulation of  $A\beta$ 1–42 dimer interacting with 10 EGCG molecules, EGCG was found buried in the interface between the  $A\beta$  peptides and bound to the hydrophobic side chain atoms of residues Phe4, Phe19/Phe20, Tyr10, Ile31/Ile32, Met35/Val36, Val39, and Ile41, and the hydrophilic N-terminal amino acids Asp1, Glu3, Arg5, Asp7, and Glu11 by H-bonds.<sup>30</sup> Via comparison with our pattern of interactions with NQTrp, the hot residues Arg5, Asp7, Tyr10, Phe19/Phe20, and Met35 are recovered, but overall, the sites with the highest interaction probability are clearly different.

Zhu et al. determined the most populated clusters of  $A\beta$ 1–42 monomer from 100 ns REMD in solvent. Then, the structures were subjected to fragment-based calculations, and they identified 35 clusters displaying binding pockets made essentially of the CHC region and residues Phe4, Tyr10, Ile31, and Met35, though hydrophilic residues can contribute, as well. The binding of curcumin and Congo red revealed that in some of the complexes, the ligands remain bound during the 80 ns MD at 300 K.<sup>58</sup> Though Tyr10, Met35, and the CHC region are identified by our study, it is not surprising to observe differences because it is well-known that the configurations of  $A\beta$ 1–42 monomer and dimer are different.<sup>17,23,59</sup>

Finally, we can compare our results with implicit solvent MD simulations of  $A\beta$ 1–42 monomer interacting with carnosine, a



dipeptide naturally occurring in the brain and rescuing cells from  $A\beta$ -induced toxicity.<sup>60</sup> Using a total MD trajectory of 3  $\mu$ s, carnosine was found to interact transiently by salt bridges with charged residues Arg5, Lys16, and Lys28, and the CHC and flanked residues. Though their binding residues differ from those identified our study, it is interesting that Arg5, Lys16, Lys28, and the CHC region are found in both studies.

## CONCLUSION

We have performed atomistic REMD simulation of the  $A\beta$ 1–42 dimer with two NQTrp molecules at a salt concentration of 150 mM. Though there are multiple binding sites, hydrophobic residues Phe19/Phe20 and Leu34/Met35 and hydrophilic residues Arg5, Tyr10, Lys16, Asp7, and Lys18 are identified as hot spots for NQTrp binding, providing therefore a different structural and dynamical picture compared to that from  $A\beta$  fragments with NQTrp. Interestingly, because all these residues are known to play a critical role in both  $A\beta$  self-assembly and toxicity, our atomistic study therefore explains the beneficial effect of the NQTrp molecule.

Using simulations, NQTrp has clearly a better binding affinity for  $A\beta$ 42 than carnosine and EGCG. At equilibrium, the population of free  $A\beta$ 42 monomers is 0% in the presence of NQTrp, while in the presence of 10 EGCG molecules, there is a population of 5.2% of free  $A\beta$ 42 monomers that would be able to associate with larger toxic and nontoxic aggregates.<sup>30</sup> Carnosine was found to be in contact with  $A\beta$ 1–42 monomer for only 20% of the simulation time at 300 K and at a concentration of 5 mM versus a concentration of 11 mM in our study.

Despite the increased affinity, the number of  $A\beta$ 42 clusters is still very high in the presence of NQTrp, reaching a total of 555, and the number of binding sites is estimated to be on the order of  $10^2$ . This result provides a picture different from that provided by standard protein–drug interaction.<sup>61</sup> While, on average, the contact surface between a small-molecule ligand and its protein receptor is 300–1000  $\text{\AA}^2$ ,<sup>62</sup> we find that the average contact surface of NQTrp with  $A\beta$ 42, calculated using all conformations, is only  $259 \pm 7.4 \text{ \AA}^2$  (with a minimum of 68  $\text{\AA}^2$  and a maximum of 396  $\text{\AA}^2$ ). Taken together, our results indicate that there is room to design more efficient drugs targeting  $A\beta$ 42 dimer against AD.

## METHODS

**Simulation.** The  $A\beta$ 1–42 sequence is DAEFRHDSGY<sup>10</sup> EVHH-QKLVFF<sup>20</sup> AEDVGSNKGK<sup>30</sup> IIGLMVGGVV<sup>40</sup> IA. The initial coordinates of  $A\beta$ 1–42 monomer were taken from model 1 of PDB entry 1IYT.<sup>63</sup> This conformation observed by NMR in an apolar environment is characterized by two  $\alpha$ -helices spanning residues 8–25 and 28–39 (Figure 1B). The monomer with the N- and C-termini treated as  $\text{NH}_3^+$  and  $\text{COO}^-$  was then replicated and translated to obtain the initial dimer structures in a parallel orientation with no interchain atomic distances of  $<10 \text{ \AA}$ . The recently developed AMBER99sb\*-ILDN force field was employed to parametrize  $A\beta$ 1–42.<sup>64,65</sup> We chose the AMBER99sb\*-ILDN force field rather than older versions of AMBER, and the OPLS-AA or GROMOS force field,<sup>66</sup> because it provides a better description of the structural and dynamical properties of well-structured proteins and allows folding of diverse proteins into their NMR structures.<sup>64</sup> The parameters for NQTrp, obtained from quantum calculations, were taken from our previous study.<sup>31</sup>

$A\beta$  dimer was initially put in the center of a dodecahedron box with periodic boundary conditions. The initial volume of the box is  $\sim 283.4 \text{ nm}^3$ . Then, two NQTrp molecules were randomly added. This molar ratio of NQTrp to  $A\beta$  matches that used experimentally.<sup>40</sup> Then, 8661

TIP3P water molecules<sup>65</sup> were added to the box. Finally, 32  $\text{Na}^+$  and 26  $\text{Cl}^-$  ions were added by randomly replacing water molecules to keep the system neutral at a physiological salt concentration of 150 mM. The pH was set to 7 with the Arg and Lys residues positively charged, the Glu and Asp residues negatively charged, and the His residues neutral with a hydrogen on the  $\epsilon$ -nitrogen site.

GROMACS (version 4.5.5)<sup>66</sup> was used. The LINCS protocol<sup>67</sup> was used to constrain the bonds involving hydrogen atoms, allowing an integration time step of 2 fs. The particle mesh Ewald method<sup>68</sup> with a cutoff of 0.9 nm was used to treat the electrostatic interactions. A cutoff of 1.2 nm was used for the van der Waals interactions. The nonbonded pair lists were updated every 0.010 ps. The coordinates were saved every 2 ps. The REMD simulation<sup>69</sup> was conducted with 64 replicas with temperature ranging from 315 to 450 K by using the method developed by Patriksson and van der Spoel.<sup>70</sup> Temperatures were controlled by the Bussi–Donadio–Parrinello velocity rescaling thermostat found to sample the canonical ensemble.<sup>71</sup> Exchanges between neighboring replicas were attempted every 2 ps, leading to an average acceptance ratio of 39.4%. The REMD simulation ran for 250 ns.

**Analysis.** The conformational entropy was calculated using the quasi-harmonic approximation.<sup>72</sup> The secondary structures of  $A\beta$  were calculated using the DSSP algorithm.<sup>73</sup> The fraction of exposed side chain surface area was calculated using the reference data presented by Miller et al.<sup>74</sup> A contact was defined if the interheavy atom distance was  $<5 \text{ \AA}$ . A hydrogen bond was considered formed when the acceptor–donor distance was not more than 3.5  $\text{\AA}$  and the acceptor–donor–hydrogen angle was not more than  $30^\circ$ . The root-mean-square deviation-based clustering method described by Daura et al.<sup>75</sup> with a cutoff of 3.5  $\text{\AA}$  for backbone heavy atoms was used to extract the representative  $A\beta$  structures. Then, for each  $A\beta$  cluster, the binding sites were obtained by analyzing all bound NQTrp molecules. The binding interfacial area was calculated as being half of the buried surface areas in the  $A\beta$ –NQTrp complex. The interaction free energy of the  $A\beta$ –NQTrp complex was estimated using the MM/PBSA method.<sup>76</sup> The data set containing 1500 snapshots was extracted from the last 150 ns at 315 K with a time interval of 100 ps. The interaction free energies between NQTrp and  $A\beta$  residues were calculated using the pairwise per-residue decomposition, with all parameters and, notably, the solvation energy taken from our previous work.<sup>30</sup> Statistical errors were estimated by block (time interval) averaging. To facilitate discussion, the N-terminal region (NT) covers residues 1–16 and the fibril-loop region (FL) spans residues 22–28.

## ASSOCIATED CONTENT

### Supporting Information

Binding sites of  $A\beta$ 1–42 clusters 11–20, lifetimes of the side chain exposed to solvent for each residue, and lifetimes of salt bridges. This material is available free of charge via the Internet at <http://pubs.acs.org>.

## AUTHOR INFORMATION

### Corresponding Authors

\*E-mail: [ygm@ntu.edu.sg](mailto:ygm@ntu.edu.sg).

\*E-mail: [philippe.derreumaux@ibpc.fr](mailto:philippe.derreumaux@ibpc.fr).

### Funding

We are grateful for the support of the French-Singapore MERLION Ph.D. 2010 program (Project 5.08.10). This work was partially supported by IDA Cloud Computing Call 4, NTU Tier 1 Grant RG 23/11, and the A\*STAR Computational Resource Centre (<http://www.acrc.a-star.edu.sg>) through the use of its high-performance computing facilities. P.D. also acknowledges financial support from ANR GRAL SIMI 12-BS07-0017, IUF, and the Pierre de Gilles Foundation.

### Notes

The authors declare no competing financial interest.

## REFERENCES

- (1) Selkoe, D. J. (2003) Folding proteins in fatal ways. *Nature* 426, 900–904.
- (2) Dobson, C. M. (2003) Protein folding and misfolding. *Nature* 426, 884–890.
- (3) Walsh, D. M., Klyubin, I., Fadeeva, J. V., Cullen, W. K., Anwyl, R., Wolfe, M. S., Rowan, M. J., and Selkoe, D. J. (2002) Naturally secreted oligomers of amyloid  $\beta$  protein potently inhibit hippocampal long-term potentiation in vivo. *Nature* 416, 535–539.
- (4) Thompson, L. K. (2003) Unraveling the secrets of Alzheimer's  $\beta$ -amyloid fibrils. *Proc. Natl. Acad. Sci. U.S.A.* 100, 383–385.
- (5) Eanes, E. D., and Glenner, G. G. (1968) X-ray diffraction studies on amyloid filaments. *J. Histochem. Cytochem.* 16, 673–677.
- (6) Kirschner, D. A., Abraham, C., and Selkoe, D. J. (1986) X-ray diffraction from intraneuronal paired helical filaments and extraneuronal amyloid fibrils in Alzheimer disease indicates cross- $\beta$  conformation. *Proc. Natl. Acad. Sci. U.S.A.* 83, 503–507.
- (7) Petkova, A. T., Ishii, Y., Balbach, J. J., Antzutkin, O. N., Leapman, R. D., Delaglio, F., and Tycko, R. (2002) A structural model for Alzheimer's  $\beta$ -amyloid fibrils based on experimental constraints from solid state NMR. *Proc. Natl. Acad. Sci. U.S.A.* 99, 16742–16747.
- (8) Lührs, T., Ritter, C., Adrian, M., Riek-Loher, D., Bohrmann, B., Döbeli, H., Schubert, D., and Riek, R. (2005) 3D structure of Alzheimer's amyloid- $\beta$ (1–42) fibrils. *Proc. Natl. Acad. Sci. U.S.A.* 102, 17342–17347.
- (9) Kirkitadze, M. D., Bitan, G., and Teplow, D. B. (2002) Paradigm shifts in Alzheimer's disease and other neurodegenerative disorders: The emerging role of oligomeric assemblies. *J. Neurosci. Res.* 69, 567–577.
- (10) Klein, W. L., Stine, W. B., Jr., and Teplow, D. B. (2004) Small assemblies of unmodified amyloid  $\beta$ -protein are the proximate neurotoxin in Alzheimer's disease. *Neurobiol. Aging* 25, 569–580.
- (11) Shankar, G. M., Li, S., Mehta, T. H., Garcia-Munoz, A., Shepardson, N. E., Smith, I., Brett, F. M., Farrell, M. A., Rowan, M. J., Lemere, C. A., Regan, C. M., Walsh, D. M., Sabatini, B. L., and Selkoe, D. J. (2008) Amyloid- $\beta$  protein dimers isolated directly from Alzheimer's brains impair synaptic plasticity and memory. *Nat. Med.* 14, 837–842.
- (12) Jin, M., Shepardson, N., Yang, T., Chen, G., Walsh, D., and Selkoe, D. J. (2011) Soluble amyloid  $\beta$ -protein dimers isolated from Alzheimer cortex directly induce Tau hyperphosphorylation and neuritic degeneration. *Proc. Natl. Acad. Sci. U.S.A.* 108, 5819–5824.
- (13) Bernstein, S. L., Dupuis, N. F., Lazo, N. D., Wyttenbach, T., Condrón, M. M., Bitan, G., Teplow, D. B., Shea, J. E., Ruotolo, B. T., Robinson, C. V., and Bowers, M. T. (2009) Amyloid- $\beta$  protein oligomerization and the importance of tetramers and dodecamers in the aetiology of Alzheimer's disease. *Nat. Chem.* 1, 326–331.
- (14) Kirkitadze, M. D., Bitan, G., and Teplow, D. B. (2002) Paradigm shifts in Alzheimer's disease and other neuro degenerative disorders: The emerging role of oligomeric assemblies. *J. Neurosci. Res.* 69, 567–577.
- (15) Kirkitadze, M. D., Condrón, M. M., and Teplow, D. B. (2001) Identification and characterization of key kinetic intermediates in amyloid  $\beta$ -protein fibrillogenesis. *J. Mol. Biol.* 312, 1103–1119.
- (16) Teplow, D. B. (2006) Preparation of Amyloid  $\beta$ -Protein for Structural and Functional Studies. In *Methods in Enzymology* (Indu, K., and Ronald, W., Eds.) pp 20–33, Academic Press, New York.
- (17) Cote, S., Laghaei, R., Derreumaux, P., and Mousseau, N. (2012) Distinct dimerization for various alloforms of the amyloid- $\beta$  protein:  $A\beta$ (1–40),  $A\beta$ (1–42), and  $A\beta$ (1–40)(D23N). *J. Phys. Chem. B* 116, 4043–4055.
- (18) Rosenman, D. J., Connors, C. R., Chen, W., Wang, C., and Garcia, A. E. (2013)  $A\beta$  monomers transiently sample oligomer and fibril-like configurations: Ensemble characterization using a combined MD/NMR approach. *J. Mol. Biol.* 425, 3338–3359.
- (19) Ball, K. A., Phillips, A. H., Wemmer, D. E., and Head-Gordon, T. (2013) Differences in  $\beta$ -strand populations of monomeric  $A\beta$ 40 and  $A\beta$ 42. *Biophys. J.* 104, 2714–2724.
- (20) Lin, Y. S., Bowman, G. R., Beauchamp, K. A., and Pande, V. S. (2012) Investigating how peptide length and a pathogenic mutation modify the structural ensemble of amyloid  $\beta$  monomer. *Biophys. J.* 102, 315–324.
- (21) Chebaro, Y., and Derreumaux, P. (2009) Targeting the early steps of  $A\beta$ 16–22 protofibril disassembly by N-methylated inhibitors: A numerical study. *Proteins: Struct., Funct., Bioinf.* 75, 442–452.
- (22) Scherzer-Attali, R., Convertino, M., Pellarin, R., Gazit, E., Segal, D., and Cafisch, A. (2013) Methylations of tryptophan-modified naphthoquinone affect its inhibitory potential toward  $A\beta$  aggregation. *J. Phys. Chem. B* 117, 1780–1789.
- (23) Melquiond, A., Dong, X., Mousseau, N., and Derreumaux, P. (2008) Role of the region 23–28 in  $A\beta$  fibril formation: Insights from simulations of the monomers and dimers of Alzheimer's peptides  $A\beta$ 40 and  $A\beta$ 42. *Curr. Alzheimer Res.* 5, 244–250.
- (24) Viet, M. H., Nguyen, P. H., Ngo, S. T., Li, M. S., and Derreumaux, P. (2013) Effect of the Tottori Familial Disease Mutation (D7N) on the Monomers and Dimers of  $A\beta$ 40 and  $A\beta$ 42. *ACS Chem. Neurosci.* 4 (11), 1446–1457.
- (25) Mitternacht, S., Staneva, I., Hard, T., and Irback, A. (2010) Comparing the folding free-energy landscapes of  $A\beta$ 42 variants with different aggregation properties. *Proteins: Struct., Funct., Bioinf.* 78, 2600–2608.
- (26) Mitternacht, S., Staneva, I., Hard, T., and Irback, A. (2011) Monte Carlo study of the formation and conformational properties of dimers of  $A\beta$ 42 variants. *J. Mol. Biol.* 410, 357–367.
- (27) Chong, S. H., and Ham, S. (2012) Atomic-level investigations on the amyloid- $\beta$  dimerization process and its driving forces in water. *Phys. Chem. Chem. Phys.* 14, 1573–1575.
- (28) Zhu, X., Bora, R. P., Barman, A., Singh, R., and Prabhakar, R. (2012) Dimerization of the full-length Alzheimer amyloid  $\beta$ -peptide ( $A\beta$ 42) in explicit aqueous solution: A molecular dynamics study. *J. Phys. Chem. B* 116, 4405–4416.
- (29) Barz, B., and Urbanc, B. (2012) Dimer Formation Enhances Structural Differences between Amyloid  $\beta$ -Protein (1–40) and (1–42): An Explicit-Solvent Molecular Dynamics Study. *PLoS One* 7, e34345.
- (30) Zhang, T., Zhang, J., Derreumaux, P., and Mu, Y. (2013) Molecular Mechanism of the Inhibition of EGCG on the Alzheimer  $A\beta$ 1–42 Dimer. *J. Phys. Chem. B* 117, 3993–4002.
- (31) Chebaro, Y., Jiang, P., Zang, T., Mu, Y., Nguyen, P. H., Mousseau, N., and Derreumaux, P. (2012) Structures of  $A\beta$ 17–42 Trimers in Isolation and with Five Small-Molecule Drugs Using a Hierarchical Computational Procedure. *J. Phys. Chem. B* 116, 8412–8422.
- (32) Meral, D., and Urbanc, B. (2013) Discrete Molecular Dynamics Study of Oligomer Formation by N-Terminally Truncated Amyloid  $\beta$ -Protein. *J. Mol. Biol.* 425, 2260–2275.
- (33) Sharoar, M. G., Shahnavaz, M., Islam, M. I., Ramasamy, V. S., Shin, S. Y., and Park, I. S. (2013) The inhibitory effects of *Escherichia coli* maltose binding protein on  $\beta$ -amyloid aggregation and cytotoxicity. *Arch. Biochem. Biophys.* 538, 41–48.
- (34) Ghanta, J., Shen, C. L., Kiessling, L. L., and Murphy, R. M. (1996) A strategy for designing inhibitors of  $\beta$ -amyloid toxicity. *J. Biol. Chem.* 271, 29525–29528.
- (35) Soto, C., Kindy, M. S., Baumann, M., and Frangione, B. (1996) Inhibition of Alzheimer's amyloidosis by peptides that prevent  $\beta$ -sheet conformation. *Biochem. Biophys. Res. Commun.* 226, 672–680.
- (36) Tjernberg, L. O., Naslund, J., Lindqvist, F., Johansson, J., Karlstrom, A. R., Thyberg, J., Terenius, L., and Nordstedt, C. (1996) Arrest of  $\beta$ -amyloid fibril formation by a pentapeptide ligand. *J. Biol. Chem.* 271, 8545–8548.
- (37) Fradinger, E. A., Monien, B. H., Urbanc, B., Lomakin, A., Tan, M., Li, H., Spring, S. M., Condrón, M. M., Cruz, L., Xie, C. W., Benedek, G. B., and Bitan, G. (2008) C-terminal peptides coassemble into  $A\beta$ 42 oligomers and protect neurons against  $A\beta$ 42-induced neurotoxicity. *Proc. Natl. Acad. Sci. U.S.A.* 105, 14175–14180.
- (38) Ehrnhoefer, D. E., Bieschke, J., Boeddrich, A., Herbst, M., Masino, L., Lurz, R., Engemann, S., Pastore, A., and Wanker, E. E.

- (2008) EGCG redirects amyloidogenic polypeptides into unstructured, off-pathway oligomers. *Nat. Struct. Mol. Biol.* 15, 558–566.
- (39) Frydman-Marom, A., Levin, A., Farfara, D., Benromano, T., Scherzer-Attali, R., Peled, S., Vassar, R., Segal, D., Gazit, E., Frenkel, D., and Ovadia, M. (2011) Orally administered cinnamon extract reduces  $\beta$ -amyloid oligomerization and corrects cognitive impairment in Alzheimer's disease animal models. *PLoS One* 6, e16564.
- (40) Scherzer-Attali, R., Pellarin, R., Convertino, M., Frydman-Marom, A., Egoz-Matia, N., Peled, S., Levy-Sakin, M., Shalev, D. E., Caflich, A., Gazit, E., and Segal, D. (2010) Complete Phenotypic Recovery of an Alzheimer's Disease Model by a Quinone-Tryptophan Hybrid Aggregation Inhibitor. *PLoS One* 5, e11101.
- (41) Necula, M., Kaye, R., Milton, S., and Glabe, C. G. (2007) Small molecule inhibitors of aggregation indicate that amyloid  $\beta$  oligomerization and fibrillization pathways are independent and distinct. *J. Biol. Chem.* 282, 10311–10324.
- (42) Pawar, A. P., Dubay, K. F., Zurdo, J., Chiti, F., Vendruscolo, M., and Dobson, C. M. (2005) Prediction of "aggregation-prone" and "aggregation-susceptible" regions in proteins associated with neurodegenerative diseases. *J. Mol. Biol.* 350, 379–392.
- (43) Scherzer-Attali, R., Shaltiel-Karyo, R., Adalist, Y. H., Segal, D., and Gazit, E. (2012) Generic inhibition of amyloidogenic proteins by two naphthoquinone-tryptophan hybrid molecules. *Proteins: Struct., Funct., Bioinf.* 80, 1962–1973.
- (44) Convertino, M., Vitalis, A., and Caflich, A. (2011) Disordered binding of small molecules to  $A\beta(12-28)$ . *J. Biol. Chem.* 286, 41578–41588.
- (45) Anand, P., Nandel, F. S., and Hansmann, U. H. E. (2008) The Alzheimer  $\beta$ -amyloid ( $A\beta_{1-39}$ ) dimer in an implicit solvent. *J. Chem. Phys.* 129, 195102.
- (46) Zhang, Y., Rempel, D. L., Zhang, J., Sharma, A. K., Mirica, L. M., and Gross, M. L. (2013) Pulsed hydrogen-deuterium exchange mass spectrometry probes conformational changes in amyloid  $\beta$  ( $A\beta$ ) peptide aggregation. *Proc. Natl. Acad. Sci. U.S.A.* 110, 14604–14609.
- (47) Yoshiike, Y., Akagi, T., and Takashima, A. (2007) Surface structure of amyloid- $\beta$  fibrils contributes to cytotoxicity. *Biochemistry* 46, 9805–9812.
- (48) Lv, X., Li, W., Luo, Y., Wang, D., Zhu, C., Huang, Z. X., and Tan, X. (2013) Exploring the differences between mouse  $mA\beta(1-42)$  and human  $hA\beta(1-42)$  for Alzheimer's disease related properties and neuronal cytotoxicity. *Chem. Commun.* 49, 5865–5867.
- (49) Ono, K., Condrón, M. M., and Teplow, D. B. (2010) Effects of the English (H6R) and Tottori (D7N) familial Alzheimer disease mutations on amyloid  $\beta$ -protein assembly and toxicity. *J. Biol. Chem.* 285, 23186–23197.
- (50) Sinha, S., Lopes, D. H. J., and Bitan, G. (2012) A Key Role for Lysine Residues in Amyloid  $\beta$ -Protein Folding, Assembly, and Toxicity. *ACS Chem. Neurosci.* 3, 473–481.
- (51) Kaden, D., Harmeier, A., Weise, C., Munter, L. M., Althoff, V., Rost, B. R., Hildebrand, P. W., Schmitz, D., Schaefer, M., Lurz, R., Skodda, S., Yamamoto, R., Arlt, S., Finckh, U., and Multhaup, G. (2012) Novel APP/ $A\beta$  mutation K16N produces highly toxic heteromeric  $A\beta$  oligomers. *EMBO Mol. Med.* 4, 647–659.
- (52) Zhang, S., Casey, N., and Lee, J. P. (1998) Residual structure in the Alzheimer's disease peptide: Probing the origin of a central hydrophobic cluster. *Folding Des.* 3, 413–422.
- (53) Zhang, S., Iwata, K., Lachenmann, M. J., Peng, J. W., Li, S., Stimson, E. R., Lu, Y., Felix, A. M., Maggio, J. E., and Lee, J. P. (2000) The Alzheimer's peptide  $A\beta$  adopts a collapsed coil structure in water. *J. Struct. Biol.* 130, 130–141.
- (54) Chen, Z., Krause, G., and Reif, B. (2005) Structure and orientation of peptide inhibitors bound to  $\beta$ -amyloid fibrils. *J. Mol. Biol.* 354, 760–776.
- (55) Ngo, S., and Guo, Z. (2011) Key residues for the oligomerization of  $A\beta_{42}$  protein in Alzheimer's disease. *Biochem. Biophys. Res. Commun.* 414, 512–516.
- (56) Ahmed, M., Davis, J., Aucoin, D., Sato, T., Ahuja, S., Aimoto, S., Elliott, J. I., Van Nostrand, W. E., and Smith, S. O. (2010) Structural conversion of neurotoxic amyloid- $\beta(1-42)$  oligomers to fibrils. *Nat. Struct. Mol. Biol.* 17, 561–567.
- (57) Bitan, G., Tarus, B., Vollers, S. S., Lashuel, H. A., Condrón, M. M., Straub, J. E., and Teplow, D. B. (2003) A Molecular Switch in Amyloid Assembly: Met35 and Amyloid  $\beta$ -Protein Oligomerization. *J. Am. Chem. Soc.* 125, 15359–15365.
- (58) Zhu, M., De Simone, A., Schenk, D., Toth, G., Dobson, C. M., and Vendruscolo, M. (2013) Identification of small-molecule binding pockets in the soluble monomeric form of the  $A\beta_{42}$  peptide. *J. Chem. Phys.* 139, 035101–035110.
- (59) Ono, K., Condrón, M. M., and Teplow, D. B. (2009) Structure-neurotoxicity relationships of amyloid  $\beta$ -protein oligomers. *Proc. Natl. Acad. Sci. U.S.A.* 106, 14745–14750.
- (60) Attanasio, F., Convertino, M., Magno, A., Caflich, A., Corazza, A., Haridas, H., Esposito, G., Cataldo, S., Pignataro, B., Milardi, D., and Rizzarelli, E. (2013) Carnosine inhibits  $A\beta(42)$  aggregation by perturbing the H-bond network in and around the central hydrophobic cluster. *ChemBioChem* 14, 583–592.
- (61) Shan, Y., Kim, E. T., Eastwood, M. P., Dror, R. O., Seeliger, M. A., and Shaw, D. E. (2011) How does a drug molecule find its target binding site? *J. Am. Chem. Soc.* 133, 9181–9183.
- (62) Smith, R. D., Hu, L., Falkner, J. A., Benson, M. L., Neroth, J. P., and Carlson, H. A. (2006) Exploring protein-ligand recognition with Binding MOAD. *J. Mol. Graphics Modell.* 24, 414–425.
- (63) Crescenzi, O., Tomaselli, S., Guerrini, R., Salvadori, S., D'Ursi, A. M., Temussi, P. A., and Picone, D. (2002) Solution structure of the Alzheimer amyloid  $\beta$ -peptide (1–42) in an apolar microenvironment. Similarity with a virus fusion domain. *Eur. J. Biochem.* 269, 5642–5648.
- (64) Lindorff-Larsen, K., Maragakis, P., Piana, S., Eastwood, M. P., Dror, R. O., and Shaw, D. E. (2012) Systematic Validation of Protein Force Fields against Experimental Data. *PLoS One* 7, e32131.
- (65) Jorgensen, W. L., Chandrasekhar, J., Madura, J. D., Impey, R. W., and Klein, M. L. (1983) Comparison of simple potential functions for simulating liquid water. *J. Chem. Phys.* 79, 926–935.
- (66) Van der Spoel, D., Lindahl, E., Hess, B., Groenhof, G., Mark, A. E., and Berendsen, H. J. C. (2005) GROMACS: Fast, flexible, and free. *J. Comput. Chem.* 26, 1701–1718.
- (67) Hess, B., Bekker, H., Berendsen, H. J. C., and Fraaije, J. (1997) LINCS: A linear constraint solver for molecular simulations. *J. Comput. Chem.* 18, 1463–1472.
- (68) Essmann, U., Perera, L., Berkowitz, M. L., Darden, T., Lee, H., and Pedersen, L. G. (1995) A smooth particle mesh Ewald method. *J. Chem. Phys.* 103, 8577–8593.
- (69) Sugita, Y., and Okamoto, Y. (1999) Replica-exchange molecular dynamics method for protein folding. *Chem. Phys. Lett.* 314, 141–151.
- (70) Patriksson, A., and van der Spoel, D. (2008) A temperature predictor for parallel tempering simulations. *Phys. Chem. Chem. Phys.* 10, 2073–2077.
- (71) Bussi, G., Donadio, D., and Parrinello, M. (2007) Canonical sampling through velocity rescaling. *J. Chem. Phys.* 126, 014101–014107.
- (72) Schlitter, J. (1993) Estimation of absolute and relative entropies of macromolecules using the covariance matrix. *Chem. Phys. Lett.* 215, 617–621.
- (73) Kabsch, W., and Sander, C. (1983) Dictionary of protein secondary structure: Pattern recognition of hydrogen-bonded and geometrical features. *Biopolymers* 22, 2577–2637.
- (74) Miller, S., Janin, J., Lesk, A. M., and Chothia, C. (1987) Interior and surface of monomeric proteins. *J. Mol. Biol.* 196, 641–656.
- (75) Daura, X., Gademann, K., Jaun, B., Seebach, D., van Gunsteren, W. F., and Mark, A. E. (1999) Peptide Folding: When Simulation Meets Experiment. *Angew. Chem., Int. Ed.* 38, 236–240.
- (76) Kollman, P. A., Massova, I., Reyes, C., Kuhn, B., Huo, S., Chong, L., Lee, M., Lee, T., Duan, Y., Wang, W., Donini, O., Cieplak, P., Srinivasan, J., Case, D. A., and Cheatham, T. E., III (2000) Calculating structures and free energies of complex molecules: Combining molecular mechanics and continuum models. *Acc. Chem. Res.* 33, 889–897.